Molecular Therapy
Methods & Clinical Development
Original Article

Expression of a CARD Slows the Retinal Degeneration of a Geographic Atrophy Mouse Model

Brianna M. Young,[1,3] Kyle Jones,[2] Michael T. Massengill,[2] Erin Walsh,[1] Hong Li,[2] Alfred S. Lewin,[2] and Cristhian J. Ildefonso[1,2]

[1]Department of Ophthalmology, University of Florida College of Medicine, Gainesville, FL 32610-0284, USA; [2]Department of Molecular Genetics & Microbiology, University of Florida College of Medicine, Gainesville, FL, USA

Age-related macular degeneration (AMD) has been linked to oxidative damage and para-inflammation, an activation of inflammasome signaling in the retinal pigment epithelium (RPE) and the underlying choriocapillaris. Herein, we tested the efficacy of a gene-delivered caspase-1 inhibitor in controlling the retinal degeneration observed in two models of RPE-choroid oxidative damage. In an acute model of oxidative stress (NaIO3 injection), eyes pre-treated with the sGFP-TatCARD (trans-activator of transcription; caspase activation and recruitment domain) vector demonstrated a recovery of retinal function and partial protection of RPE structure 1 month after damage, in contrast with control-treated eyes. In a model of chronic oxidative stress (RPE-specific deletion of *Sod2*), eyes treated with the sGFP-TatCARD vector after the onset of degeneration had a significantly slower decline in retinal function when compared to control-treated eyes. Earlier treatment of this model with the same adeno-associated virus (AAV) vector resulted in a greater protection of RPE function in eyes treated with the TatCARD when compared to control-treated eyes. Our results demonstrate that intravitreal delivery of sGFP-TatCARD reduces inflammation and can protect the retina from both acute and sustained oxidative damage within the RPE and choroid. Therefore, gene therapy with a cell-penetrating inflammasome inhibitor such as CARD may stem the progression of AMD.

INTRODUCTION

Retinal degenerative diseases are characterized by a progressive loss of light-sensitive photoreceptor cells within the retina, leading to vision impairment and, in certain diseases, complete blindness. Genetic abnormalities are known to be the main causes of retinitis pigmentosa (RP), while in other diseases, such as age-related macular degeneration (AMD), genetic variation accounts for an increased risk of disease development. In both of these diseases, however, the inflammation is increased in late stages of the disease.[1,2] More specifically, activation of the inflammasome-signaling pathway within certain cells of the retina has been shown to occur in both RP and AMD.[3,4] Thus, identifying a therapeutic intervention that can inhibit the activity of this pro-inflammatory pathway may mitigate the disease progression.

AMD is the most common cause of visual impairment in developed countries among individuals 65 years and older.[5] Early stage AMD is characterized by macular deposits called drusen that are visible in routine ophthalmoscopic examination. These protein- and lipid-rich deposits lie between the retinal pigment epithelium (RPE) and the choroid, which provides the blood supply to the photoreceptor cells of the retina. There are two advanced forms of this disease, known as neovascular AMD (nAMD) and geographic atrophy (GA). Currently, there is US Food and Drug Administration (FDA)-approved therapy for managing nAMD involving recurrent injections of monoclonal antibodies or soluble receptors. Unfortunately, there is no effective treatment for GA. AMD is a multifactorial disease linked to environmental factors, such as smoking, and genetic predisposition, such as specific variants like rs10922109 in the *CFH* region and rs2284665 in the *ARMS2-HTRA1* region.[6] The CFH risk allele and the accumulation of complement proteins in drusen implicate dysregulation of the alternative complement cascade in AMD pathogenesis. AMD has also been associated with an increase in oxidative stress within the RPE layer.[7] Other observations from patient samples have linked the disease to a slow and chronic process of inflammation[8,9,10,11] known as para-inflammation.

The inflammasome-signaling pathway is part of the repertoire of pattern recognition receptors (PRRs) of the innate immune system. These receptors can recognize either pathogen-associated molecular patterns (PAMPs) or danger-associated molecular patterns (DAMPs), and as a result they induce the activation and secretion of pro-inflammatory cytokines such as interleukin-1 beta (IL-1β) and IL-18. Within the retina, the most studied inflammasome receptor

Received 19 December 2018; accepted 6 June 2019;
https://doi.org/10.1016/j.omtm.2019.06.001.

[3]Present address: Trinity School of Medicine, Trinity College Road, Ribishi VC0100, St. Vincent and the Grenadines

Correspondence: Cristhian J. Ildefonso, PhD, Department of Ophthalmology, University of Florida College of Medicine, P.O. Box 100284, Gainesville, FL 32610-0284, USA.
E-mail: ildefons@ufl.edu

is the nucleotide-binding oligomerization domain, Leucine rich repeat, and Pyrin domain-containing (NLR) family pyrin-containing 3 (NLRP3) receptor, which localizes within the cytoplasm of the cells and can sense DAMPs and changes in oxidative stress.[12–14] When engaged by its ligand, the receptor associates with the apoptosis-associated speck-like protein containing a caspase activation and recruitment domain (CARD) (ASC), which then recruits the inflammatory pro-caspase-1 and induces its conversion into its active form. The elucidation of this inflammasome structure in 2014 demonstrated that each active inflammasome contains several filaments of active caspase-1, indicating the critical role of caspase-1 in the amplification of this signaling pathway.[15] Thus, targeting caspase-1 to control overactive inflammasome signaling in a pathological setting could be of great clinical value.

Our group has previously developed and characterized a free-form of the CARD that has been designed to be secreted and cell penetrating.[16] This molecule can be delivered as a gene construct using an adeno-associated virus (AAV) vector containing four tyrosine-to-phenylalanine capsid mutations and a tyrosine-to-valine mutation within the capsid proteins. This AAV2quad(Y-F) + T491V mutant capsid allows the efficient transduction of retinal ganglion cells and bipolar cells, but not photoreceptor cells or the RPE, after an intravitreal injection in mice.[17] This AAV2quad(Y-F) + T491V delivering a secretable GFP (sGFP) fused to a trans-activator of transcription (Tat)CARD through a furin cleavage site was shown to inhibit IL-1β production and decrease the number of infiltrative cells in a mouse model of endotoxin-induced uveitis.[16] Furthermore, the expression of this vector did not affect the structure or the function of the mouse retina, thus suggesting that targeting this pathway within the retina could be safe *in vivo*.

In this study, we evaluated the effects of inhibiting caspase-1 activation within the retina of two mouse models of RPE oxidative damage. In the first model, we induced RPE oxidative damage with a systemic injection of sodium iodate, leading to an acute and selective destruction of the RPE due to increases in oxidative stress.[18] In our second model, we induced genetic deletion of the manganese superoxide dismutase (MnSOD encoded by *Sod2*) within the RPE of C57BL/6J mice carrying a tetracycline-induced Cre-recombinase controlled by the RPE-specific promoter VMD2. Mice with an *Sod2*floxed::VMD2Cre+ genotype were fed doxycycline from post-natal day (P)0 to P14 to induce the genetic deletion of exon 3 of *Sod2*. These mice exhibit damage to the choroid and Bruch's membrane and develop slow and progressive retinal degeneration based on structural and functional studies.[19] We have now also demonstrated an inflammatory process develops in the aging retina of these mice. Furthermore, treatment of these mice with our AAV vector delivering the secretable and cell-penetrating CARD resulted in a decreased progression of retinal function decline. This effect takes place without any significant structural protection of the outer nuclear layer or the RPE structure, thus suggesting that surviving photoreceptors remain functional even in the presence of damaged RPE.

RESULTS

Expression of TatCARD Allows Retinal Function Recovery after Acute Oxidative Damage to the RPE

The sodium iodate (NaIO3) retina mouse model is an induced model of acute RPE oxidative damage[20–23] that has been previously used to study the effects of oxidative stress in the retina. To study the effects of caspase-1 inhibition within the retina during an event of acute oxidative stress, we injected C57BL/6J mice intravitreally with an AAV2quad(Y-F) + T491V (Y272F + Y444F + Y500F + Y730F + T491V) vector delivering either GFP or sGFP-TatCARD under the control of the small chicken beta-actin promoter (smCBA). Then 1 month later, mice were injected intraperitoneally with 25 mg/kg NaIO3 to induce RPE oxidative damage.

These mice were evaluated at 1, 2, and 4 weeks after NaIO3 by electroretinography (ERG) to study the electrical response of the retina to light. When we compared the average amplitudes of a-wave (photoreceptor cells), b-wave (bipolar cells), or c-wave (RPE) between 1 week before NaIO3 injection and 1 or 2 weeks after injury, we found that both GFP- and sGFP-TatCARD-treated eyes showed a significant decrease (Figures 1A–1C). However, when the same mice were evaluated at 4 weeks after NaIO3 injection, the amplitudes of the AAV-GFP-treated eyes continued to decrease, while eyes treated with sGFP-TatCARD had a recovery of their ERG amplitudes and were at least twice the amplitude of the control-treated eyes for each component of the ERG response (Figures 1A–1C).

To assess structural recovery, we used flat-mount staining with ZO-1 (a marker of tight junctions) within the RPE of eyes injected with AAV vector delivering either GFP or sGFP-TatCARD. Our images indicate that eyes treated with AAV-GFP had a greater structural damage of the RPE when compared to eyes treated with AAV-sGFP-TatCARD (Figure 1D). As a comparison, we stained flat mounts of mice that were not treated with NaIO3 to show a normal ZO-1-stained flat mount. When the damaged area for each image was quantified and standardized to the overall area of the flat mounts, we observed a statistically significant reduction in the damaged area in eyes treated with sGFP-TatCARD when compared to GFP-treated eyes (Figure 1E).Together these results suggest that the expression of TatCARD in the retina allows recovery after an acute event of RPE oxidative damage.

Knockdown of SOD2 Induces the Activation of IL-1β *In Vitro*

To test the correlation between oxidative stress and inflammasome activation, we suppressed the expression of MnSOD (also known as SOD2, a key antioxidant enzyme) using small interfering RNA (siRNA) transfection in ARPE-19 cells. This cell line is a spontaneously derived RPE cell line that is commonly used to study RPE function. While a recent report indicates that this cell line does not express NLRP3,[24] activation of caspase-1 by other inflammasomes and secretion of IL-1β have been reported in primary human RPE cells.[25] Cells were transiently transfected with either a control siRNA (Ctrl siRNA) or an *SOD2* siRNA set (*SOD2* siRNA). We detected the knockdown of

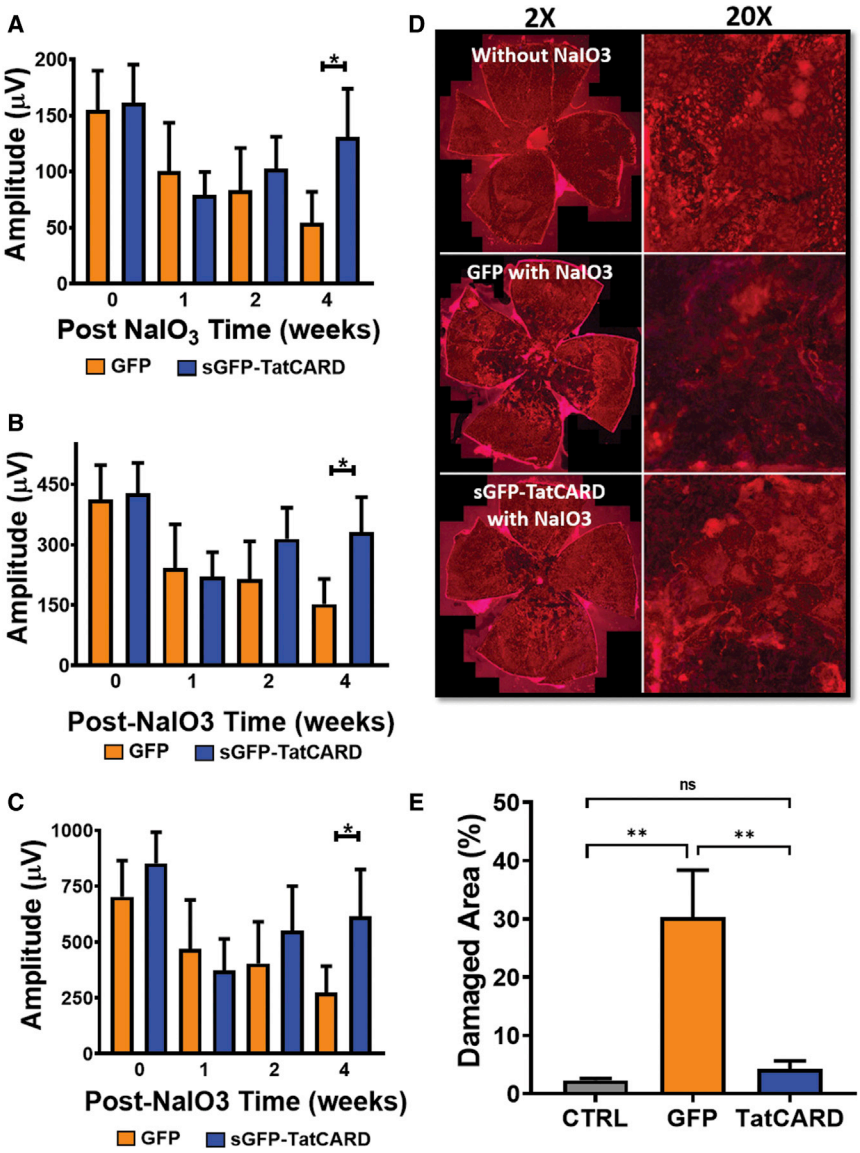

Figure 1. Intravitreal Administration of AAV2quad (Y-F) + T491V Delivering sGFP-TatCARD Allows Retina Function Recovery after an Acute RPE Oxidative Damage Insult

(A–C) Mice received an intravitreal injection of AAV2quad (Y-F) + T491V vector delivering either GFP or sGFP-TatCARD, and they were evaluated by electroretinography (ERG) at 1 month post-injection (0) and one (1), two (2), and four weeks (4) after an intraperitoneal injection of NaIO3 (25 mg/kg). Values graphed represent the average amplitudes of their a-wave (A), b-wave (B), and c-wave (C). Although average amplitudes decreased from 0 to 2 weeks post-NaIO3 injection, only eyes treated with the sGFP-TatCARD vector had a significant recovery of their ERG amplitudes at 4 weeks after the NaIO3 injection. (D) Flat mounts stained with ZO-1 from eyes 4 weeks after a systemic injection of NaIO3. Eyes treated with the sGFP-TatCARD vector had more ZO-1 staining (better RPE morphology) when compared to GFP vector-treated eyes. (E) Total area of flat mount and damaged areas were quantified for each sample. Values are reported as percents of damaged area ([damaged area/total area]*100). Samples treated with TatCARD had a statistically significantly lower percent of damaged area when compared to GFP-treated samples. As a control, we used a flat mount from a non-injected mouse stained with ZO-1. Values are reported as average ± SEM (n = 5 mice). *$p \leq 0.05$, **$p \leq 0.01$.

MnSOD by western blot and quantified the relative knockdown using ImageJ software. The siRNA transfection resulted in an 80% knockdown of SOD2 protein (Figure 2A).

Using the same siRNA, we then performed an ELISA to quantify the concentration of secreted IL-1β in the medium of transfected cells. The knockdown of *SOD2* mRNA in ARPE-19 cells resulted in a significant increase in the secretion of IL-1β when compared to medium from control siRNA-transfected cells (Figure 2B). These results suggest that knockdown of SOD2 in RPE-like cells results in the activation of the inflammasome-signaling pathway.

In 2014, Mao et al.[26] described a genetic model of GA that induces the conditional deletion of Sod2 within the RPE layer of C57BL/6J mice. These mice had a significant decrease in their outer nuclear layer (ONL), a decline in their electroretinogram a- and b-wave functions, and an increase in mosaic presence of oxidative stress markers within their RPE layer.[27] To further validate the damage to the RPE of this mouse model, we measured the c-wave as well as the a- and b-wave functions. The c-wave amplitude is a positive deflection following the b-wave amplitude of a greater magnitude, known to be a response of the RPE to a light stimulus, which depends on the health of these cells.[28] We have validated such a-wave and b-wave decline, and we observed a similar decrease in the c-wave function of these animals, as demonstrated in Figure 2C. Furthermore, we also have shown that this mouse model has a decline in the c-wave amplitude, which is directly associated with the function and health of the RPE. When we aged these animals up to 9 months, we observed the presence of vacuoles within the RPE, basal laminal deposits, and disorganization of photoreceptor outer and inner segments (Figure 2D) in electron microscopy micrographs. These results indicate that the RPE-specific Sod2-knockout (KO) mouse model recapitulates certain features of GA and can serve as an animal model of the disease.

Genetic Deletion of Sod2 within the RPE Leads to a Slow and Progressive Inflammatory Response

There is no animal model of GA that recapitulates all the clinical features of the human disease. Previously, we have used the RPE-specific

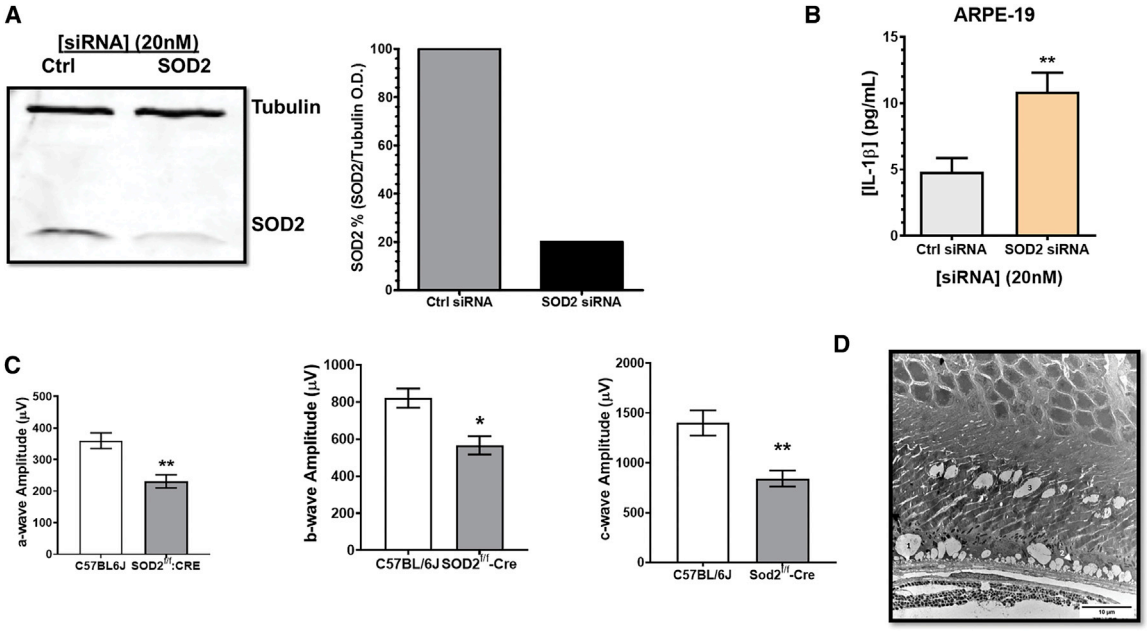

Figure 2. Knockdown of SOD2 Induces the Activation of Caspase-1 *In Vitro*

(A) ARPE-19 cells were transiently transfected with either control (Ctrl) or SOD2 siRNA. Expression of SOD2 was detected by western blot 48 h after transfection. Expression of SOD2 was quantified using tubulin band intensity as a control. Cells transfected with the SOD2 siRNA had ~80% knockdown of Sod2 protein levels. (B) The conditioned media of transfected cells were used to quantify the concentration of secreted IL-1β, a caspase-1-regulated cytokine. The concentration of IL-1β was quantified by ELISA. Cells transfected with SOD2 siRNA had on average a 2-fold increase in the concentration of IL-1β in their medium when compared to cells transfected with Ctrl siRNA. (C) Amplitudes of a-, b-, and c-waves of 12-week-old C57BL/6J and Sod2f/f-Cre mice. Sod2f/f-Cre mice had a statistically significant decrease in all amplitudes when compared to C57BL/6J mice. (D) Electron microscopy micrograph of a 9-month-old Sod2f/f-Cre mouse showing RPE vacuoles (1), lipofuscin accumulation (2), and damaged photoreceptors (3). Values are reported as average ± SEM (n = 6 samples from 2 independent transfections). *$p \leq 0.05$, **$p \leq 0.01$.

Sod2-KO (*Sod2*tg) mouse model described by Mao et al.[26] In this model, doxycycline feeding leads to the genetic deletion of exon 3 of the *Sod2* gene within the RPE, and this leads to a slow functional and structural degeneration associated with increases in oxidative stress markers.[29] Specifically, the functional decline in the retina of these mice starts between 4 and 5 months of age.[26]

To determine if the *Sod2* deletion within the RPE leads to an inflammatory response, we stained the retinas of 9-week-old mice with anti-glial fibrillary acidic protein (GFAP) and with anti-IL-1β antibodies (Figure 3A, top row). GFAP is induced in activated Müller glia and astrocyte cells, while IL-1β is produced in retinal cells, including microglia and RPE cells. These retinas sections had minimal GFAP and IL-1β staining, suggesting that, at this time point, the deletion of *Sod2* within the RPE did not result in an inflammatory response. Since this mouse model starts manifesting characteristics of retinal degeneration between 4 and 6 months old, we decided to evaluate the retinas of 25-week-old animals. Mice of this age showed increased IL-1β staining (Figure 3A, bottom row) and a concomitant increase in gliosis (GFAP staining) in contrast to the 2-month-old animals.

To supplement our immunohistochemistry, we used multiplex ELISA technology to quantify the concentration of multiple cytokines and chemokines in the retinas of these mice. As a control, we used mice carrying the floxed *Sod2* gene but no *VMD2Cre*, which is required for the deletion of *Sod2*. Although we measured the absolute concentration of these molecules (Figure S1), we standardized each concentration to that quantified in 8-week-old *Sod2*tg mice. Our results demonstrate that, at 8 weeks of age, there were no significant differences between the *Sod2*tg and Sod2flx mice lacking the expression of Cre in the concentrations of the many common chemokines and cytokines associated with an inflammatory response (Figure 3B). However, by 10 weeks, our mouse model showed increases in IL-1α, IL-1β, IL-2, IL-9, IL-15, and tumor necrosis factor alpha (TNF-α) (Figures 3B and 3C), which are cytokines associated with the activation of the innate (IL-1α, IL-1β, and TNF-α) and the adaptive (IL-2 and IL-9 secreted by T cells) immune systems. Together, these results suggest that, at least at 10 weeks of age, the RPE-specific deletion of *Sod2* initiated an inflammatory response within the retina of this mouse model of GA.

At 25 weeks, the levels of TNF-α and IL-9 were somewhat lower than at 10 weeks, but IL-1α and IL-2 remained elevated, and higher levels of IL-15 (Figure 3C), which shares many properties with IL-2, and Monokine induced by gamma interferon (MIG; CXCL9) were detected. CXCL9 is involved in T cell recruitment, and it is elevated in the retinas of light-challenged C57BL/6J mice.[30] Taken together, these results demonstrate that our mouse model of GA not only

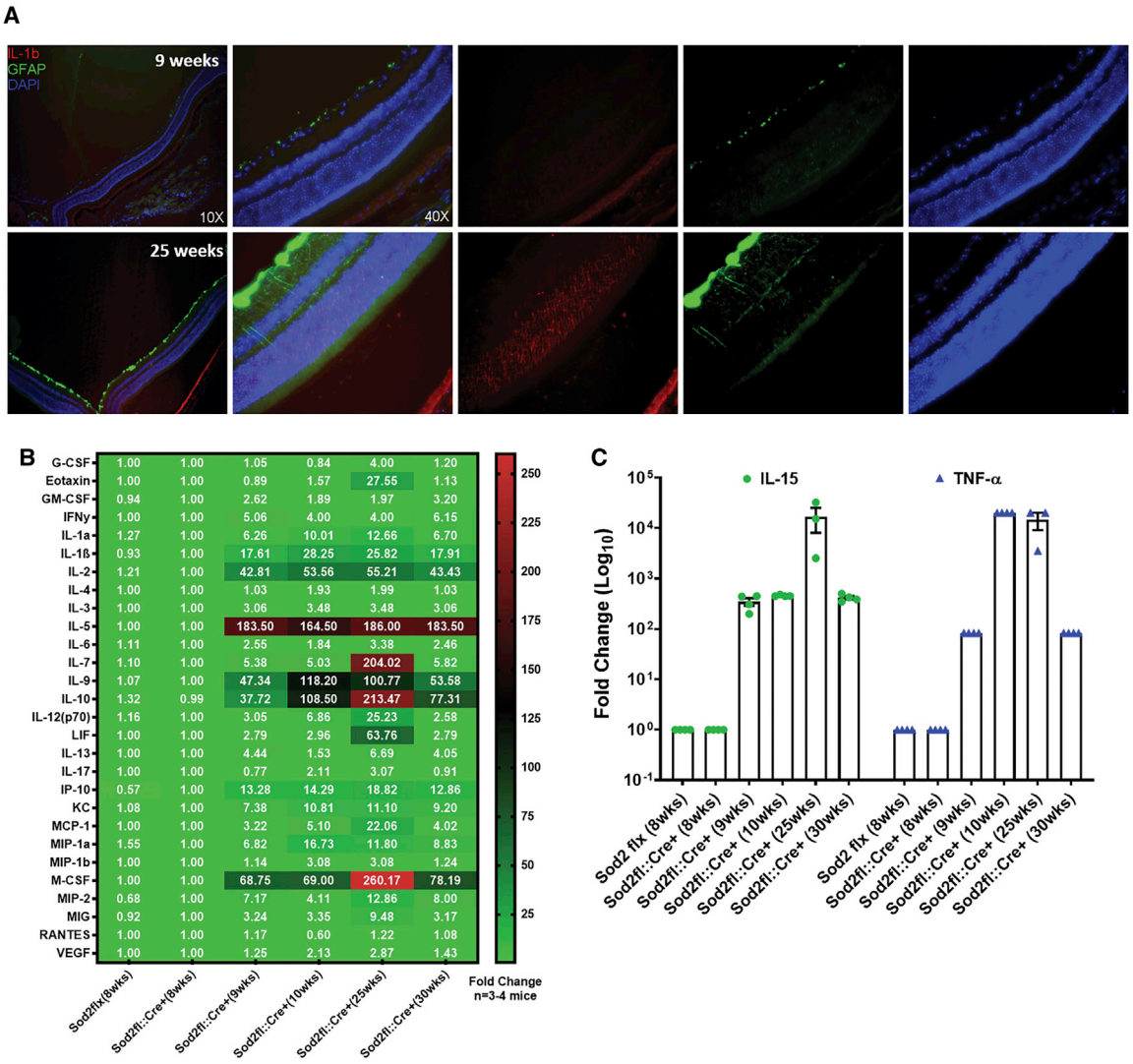

Figure 3. The *Sod2*^{floxed}*::VMD2*$^{Cre+}$ Mice Develop a Retina Inflammation with Aging

Mice carrying a floxed SOD2 exon 3 were crossed to mice carrying the Cre recombinase under the regulation of the RPE-specific VMD2 promoter. The *Sod2floxed::VMD2Cre+* progeny was confirmed by PCR genotyping and fed doxycycline chow from P0 to P14. (A) Mice were euthanized at 10 and 24 weeks of age, and their eyes were harvested for immunofluorescence staining against GFAP. At 10 weeks of age, there was minimal GFAP-positive staining, and it was limited to the retina nerve fiber layer; however, there was a more pronounced staining observed at 24 weeks of age, with staining spanning from the retina nerve fiber layer (RNFL) toward the ONL of the retina. (B) Quantification of cytokines and chemokines within the retina lysates of these mice was done using multiplex ELISA. Analyte values represent the fold changes over that of the 8-week-old Sod2fl::Cre+ amount of specific molecule. Analyte concentrations were standardized to total amount of protein used in the assay (pg/mg total protein). (C) Fold changes of IL-15 and TNF-α. Values are reported as average ± SEM (n = 3–4 mice).

has markers of oxidative stress but also of a chronic inflammatory process that occurs with aging.

Retinal Expression of TatCARD Significantly Decreases IL-1β Expression in the Retina of RPE-Specific Sod2-Deleted Mice

The 4-month-old mice carrying the RPE-specific deletion of *Sod2* were injected intravitreally with 3×10^{10} vector genome copies of AAV2quad(Y-F) + T491V vector delivering either GFP or TatCARD. We harvested their eyes at 18 months of age to determine the expression of IL-1β in their retinas. These eyes were also stained with antibodies against markers of gliosis (GFAP and Iba1). We observed more IL-1β cells in the inner layers of the retina in eyes treated with GFP control when compared to TatCARD-treated eyes (Figure 4A). Using these images, we quantified the fluorescence intensity of IL-1β and DAPI staining to compare the effects of TatCARD treatment with those of the GFP control. Our results indicated that the expression of IL-1β in the retinas of TatCARD-treated eyes was significantly decreased when compared to that of GFP control-treated eyes

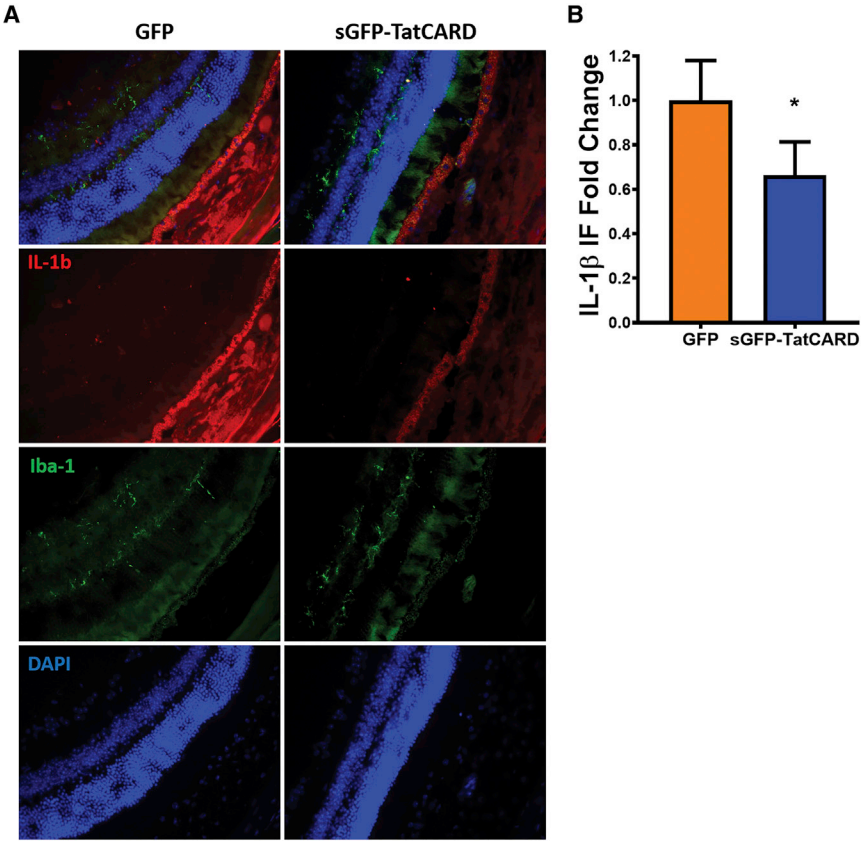

Figure 4. Intravitreal Administration of AAV2quad (Y-F) + T491V/smCBA-sGFP-TatCARD Decreases IL-1β in the Retinas of Aged *Sod2*tg Mice

Eyes from 18-month-old Sod2-knockout mice treated with AAV vector, delivering either sGFP-TatCARD or GFP, were harvested and stained with antibodies against IL-1β and Iba1. (A) Representative images of retinal sections from sGFP-TatCARD- and GFP-treated eyes. Images for each staining were obtained and an overlay is provided on top of the montage. (B) Quantification of IL-1β (red channel) and DAPI (blue channel) fluorescence intensity from images. Fluorescence intensity for each sample was standardized to its corresponding DAPI staining, and the fold change was calculated using the signal for GFP-treated samples. The fluorescence intensity of IL-1β was significantly lower among eyes treated with sGFP-TatCARD-delivering vector when compared to GFP-treated eyes. Values are reported as average ± SEM (n = 8 images). *$p \leq 0.05$.

(Figure 4B). Together these results suggest that our TatCARD vector decreases IL-1β expression in the retina of the RPE-specific *Sod2*-deleted mouse model of GA.

AAV-TatCARD Slows the Retinal Degeneration Associated with the RPE-Specific Sod2 Deletion

We administered 3×10^{10} vector genome copies of AAV2quad (Y-F) + T491V expressing TatCARD or GFP by intravitreal injection to 4-month-old *Sod2*tg mice. This was a single-stranded AAV vector, and expression was directed by the CBA promoter. Mice were injected bilaterally, with each mouse receiving therapeutic vector (TatCARD) in one eye and control vector (GFP) in the contralateral eye. These mice were followed longitudinally by ERG to asses if retinal expression of TatCARD prevented the retinal degeneration in this mouse model. Between 6 and 9 months of age, this cohort of mice displayed a similar pattern of functional decline of their photoreceptors (Figure 5A), bipolar cells (Figure 5B), and RPE cells (Figure 5C) in both GFP- and sGFP-TatCARD-treated retinas. However, at 14 and 18 months, there was a significant protection of all the electroretinogram amplitudes in retinas expressing sGFP-TatCARD when compared with GFP-expressing retinas. A representative wave form showing the a-wave, b-wave, and c-wave responses at 18 months is shown in Figure 5D. These animals had no significant difference between GFP and sGFP-TatCARD treatments in the implicit time for any of the wave amplitudes (Figures S2A–S2C). These results suggest that, although TatCARD expression did not stop the functional retinal degeneration of this mouse model, it reduced the rate of degeneration at later stages of the progression.

To test if an earlier intervention with the TatCARD gene would result in a more pronounced protection of the retina function, we intravitreally injected a second cohort of 2-month-old *Sod2*tg mice with the same dose of AAV2quad(Y-F) + T491V delivering either GFP or sGFP-TatCARD in the contralateral eye. Mice were evaluated by ERG to detect changes in their retinal function. Earlier intervention did not significantly protect the a-wave amplitudes reflecting photoreceptor function (Figure 6A), but it led to a significant increase in the b-wave amplitudes reflecting the function of second-order neurons (Figure 6B). There was also an increase in the c-wave amplitudes, indicating improved RPE channel activity (Figure 6C). Once more, we did not observe a significant difference in the implicit time for the wave amplitudes between GFP and sGFP-TatCARD groups (Figures S2D–S2F). At 18 months, we could observe a more pronounced protection of the c-wave when compared to all the other amplitudes (Figure 6D).

Retinal Expression of TatCARD within the Retina of the RPE-Specific Sod2-KO Mice Partially Protects the Retina Structure

To determine if the protection of the retina function quantified by ERG correlates with a protection of the retina structure, we also evaluated animals treated at 2 months of age using spectral domain optical coherence tomography (SD-OCT). The nuclei of all the photoreceptors lie within the ONL; thus, we measured the total thickness of the retina and the thickness of the ONL. When we compared the average total retina thickness between sGFP-TatCARD- and GFP-treated eyes, we found that there was a statistically significantly thicker retina in the sGFP-TatCARD-treated eyes (Figures 7A and

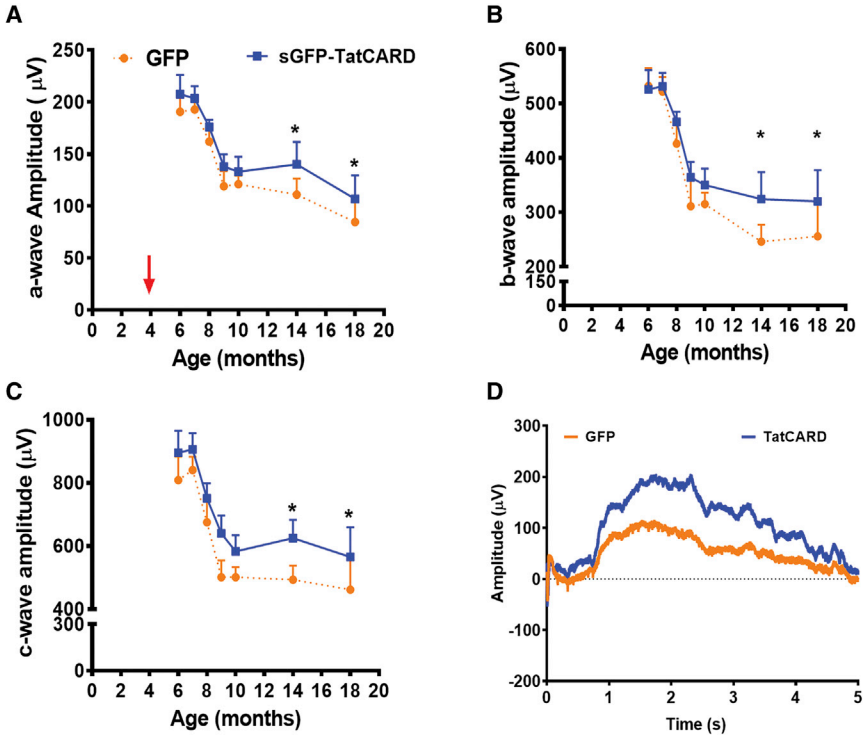

Figure 5. Administration of AAV2quad(Y-F) + T491V Delivering sGFP-TatCARD Slows the Functional Degeneration Associated with the RPE-Specific Deletion of Sod2

(A–C) Mice of the Sod2floxed::VMD2Cre+ genotype were fed doxycycline for 14 days after birth. Mice were administered 3 × 10^{10} vector genome copies (vgc) AAV2quad(Y-F) + T491V vector delivering either GFP or sGFP-TatCARD at 4 months of age (red arrow). Mice were followed by ERG until 18 months of age. Average ± SEM a-wave (A), b-wave (B), and c-wave (C) amplitudes are reported. (D) Representative ERG response of a mouse treated with TatCARD and GFP at 18 months of age. *p ≤ 0.05, n = at least 8 mice.

7B). However, when we compared the average thickness of the ONL between these groups, the difference between the sGFP-TatCARD-treated eyes and the GFP-treated eyes did not reach statistical significance (Figure 7C).

To determine which retinal layer was responsible for the significant difference in the total retina thickness, we measured the thicknesses of the inner, middle, and outer retina using segmentation software developed by Bioptigen (Figure 7D). Our results indicated that the inner retina thickness was significantly greater in the TatCARD-treated eyes when compared to GFP-treated eyes. Furthermore, the inner nuclear layer (INL) (which contains the nuclei of the second-order neurons of the retina) was significantly thicker in the TatCARD-treated eyes when compared to the GFP group. The group of mice treated with TatCARD at 2 months of age showed no preservation of a-wave amplitude but a significant increase in b-wave amplitude, reflecting the function of the bipolar cells. This maintenance of inner retina function corresponds to the relative preservation of INL structure, as reflected in the total retinal thickness.

To support our SD-OCT observations, we evaluated the retina structure by histology using plastic sections. We used imaging processing to quantify the number of nuclei within both the ONL and INL in these sections. This method has been utilized to characterize retinal degeneration in other animals.[31,32] Our results confirmed the conclusion of the SD-OCT analysis that there was no statistically significant difference in the number of photoreceptor nuclei within the ONL of our specimens from the two treatment groups (Figures 8A and 8B).

Similarly, when we quantified the number of nuclei within the INL layer, we found that there was a significantly greater number of nuclei in the eyes treated with TatCARD compared to GFP treatment in the inferior hemisphere (Figure 8C). We then used electron microscopy (EM) to study changes in cellular structures within these samples. In both GFP- and sGFP-TatCARD-treated retinas, we observed the presence of RPE vacuoles and basal laminar deposits (Figure 8D). In contrast, retinas treated with sGFP-TatCARD displayed more organized photoreceptor inner segments and denser nuclei within the ONL. These results suggest that, although there was a preservation of the total retina thickness, such effect was not due to an overall preservation of photoreceptors but to the partial preservation of the second-order neurons in the retina.

DISCUSSION

Using two mouse models of GA, we have tested a secretable and cell-penetrating caspase-1 inhibitor that can be delivered to the retina using an AAV vector. In the sodium iodate model of acute RPE injury, pre-treatment with TatCARD did not prevent injury, but it allowed recovery from damage, as indicated by increasing ERG amplitudes (Figure 1). The continued decrease in ERG response in control-treated mice suggests that the long-term injury is associated with an inflammatory response to the initial oxidative injury. Indeed, Xiao and colleagues[33] have recently shown an influx of Iba1-positive monocytic cells in the outer retinas of rats treated systemically with NaIO3. This group also showed that preventing cell death, with a peptide antagonist of the Fas receptor, reduced the infiltration of immune cells.

We also tested AAV-sGFP-TatCARD in a slow progressive model of RPE oxidative stress. Measurement of cytokine and chemokine profiles in this model indicated an increase in inflammatory markers by 10 weeks of age, which began to resolve by 30 weeks of age even without treatment (Figure 3B). AAV-sGFP-TatCARD was able to slow the functional degeneration that is characteristic of this model. Structurally, this AAV vector managed to maintain the retina

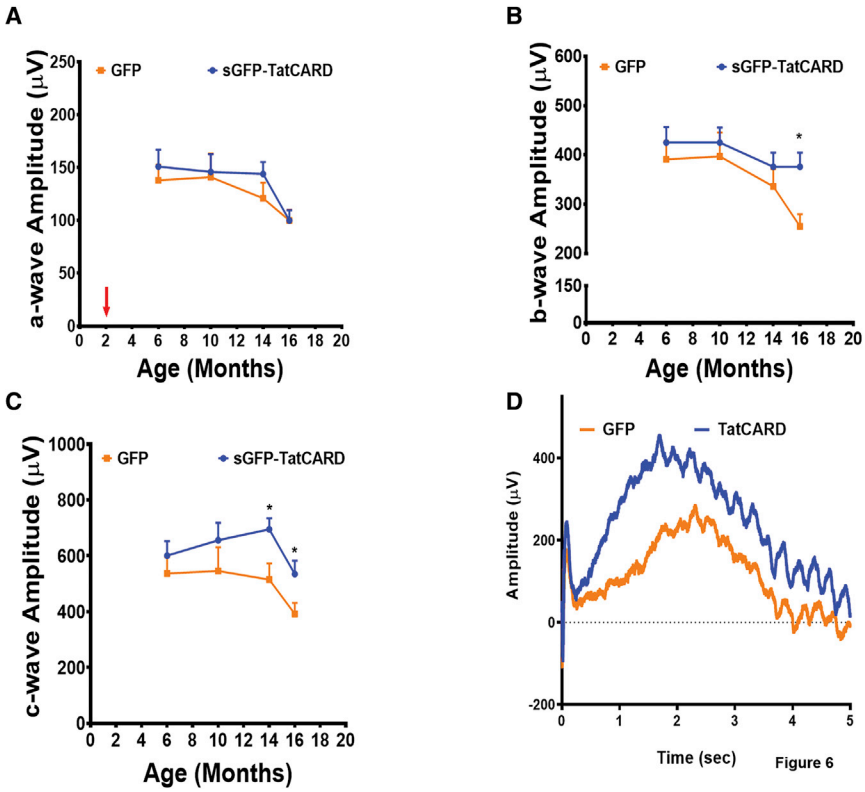

Figure 6. Early Intervention with the AAV2quad (Y-F) + T491V/smCBA-sGFP-TatCARD Does Not Significantly Improve the Function of the *Sod2*tg Retina Mice

SOD2floxed::VMD2Cre+ mice were fed doxycycline from P0 to P14. Mice were injected intravitreally with 3×10^{10} vgc AAV2quad(Y-F) + T491V delivering either GFP or sGFP-TatCARD at 2 months of age (red arrow). Mice were evaluated by ERG for 16 months. Average ± SEM a-wave (A), b-wave (B), and c-wave (C) amplitudes were compared between GFP- and sGFP-TatCARD-treated eyes. (D) Representative ERG response of a mouse treated with GFP and TatCARD at 16 months of age. *$p \leq 0.05$, n = at least 8 mice.

thickness, which was decreased in the control-treated eyes. The vector was administered at 4 months of age, but functional protection was observed only between the ages of 9 and 18 months. Since the rate of ERG decline was similar between treatment groups for the first 4 months following intravitreal injection, we conclude that, in this model also, reducing inflammasome signaling does not mitigate the oxidative damage to the retina and RPE. Increased ERG responses among aging mice, however, suggest that the inhibition of caspase-1 protects retinal function from an inflammatory response to oxidative insult.

Activation of the NLRP3 inflammasome has been linked to AMD.[34] This pathway leads to the processing of pro-IL-1β and pro-IL-18 into their mature forms and to their secretion. This processing is mediated by the caspase-1 enzyme, which, upon recruitment to the inflammasome complex, self-cleaves and becomes polymerized into long filamentous arms.[15] Interfering with the recruitment and activation of caspase-1 into the inflammasome complex thus would have tremendous effects on the production of both inflammatory cytokines. Kosmidou et al.,[24] using rigorously validated antibodies, found that the NLRP3 protein is not expressed in primary human RPE cells or in ARPE-19 cells, even following pro-inflammatory stimuli. Not all inflammasome complexes rely on NLRP3 as an intracellular receptor, however. Using primary human RPE cells, Bian and co-workers[25] showed that CD40L induces the activation NALP1 and NALP3 inflammasomes in primary human RPE cells, leading to cleavage of caspase-1 and caspase-5 and to IL-1β and IL-18 secretion. Since the soluble CARD we introduced using the AAV binds directly to caspase-1,[16] it should be capable of blocking caspase activation, regardless of which Nod-like receptor is involved.

Nevertheless, the slow kinetics of protection by AAV-sGFP-TatCARD suggest that glial cells, and not the RPE, may be the primary target of inflammasome inhibition in the models we have employed. In the RPE-specific *Sod2*-KO mice, we did not prevent the decline in retinal function between 4 and 8 months, but we reduced the decline thereafter. It was only after the stage at which the migration of monocytic cells (Iba1 positive) and activation of Müller glia (GFAP positive) were detected that the treatment exerted its effect. This timing suggests that TatCARD is dampening inflammatory cytokines released by responding glial cells at later stages of the injury and, thus, mitigating damage.

AMD is a multifactorial disease. It has been linked to oxidative stress within the RPE layer, dysregulation of the complement within the retina, and activation of pro-inflammatory signals. Due to this complexity, there is no animal model of GA that recapitulates all the clinical signs and pathological features of the human disease; instead, different models are currently being used to study the disease and develop therapies.[35] Herein we have demonstrated that our RPE-specific *Sod2*-KO mouse model of GA not only develops oxidative stress, as described originally, but also develops an inflammatory response. This response occurs with aging, which makes our model similar to the human disease.

Gene delivery in the retina using AAV vectors has been demonstrated not only to be safe in humans but also to be effective for retinal degenerative diseases such as LCA2.[36] This has led to the FDA approval of LUXTURNA, the first AAV vector-based therapy for Leber's congenital amaurosis (LCA). The success of this therapy resides in the monogeneic cause of the disease: mutations in the RPE65 gene are the cause of this disease. Unfortunately, for many other retinal degenerative diseases, the pathophysiological cause of the disease is multigeneic

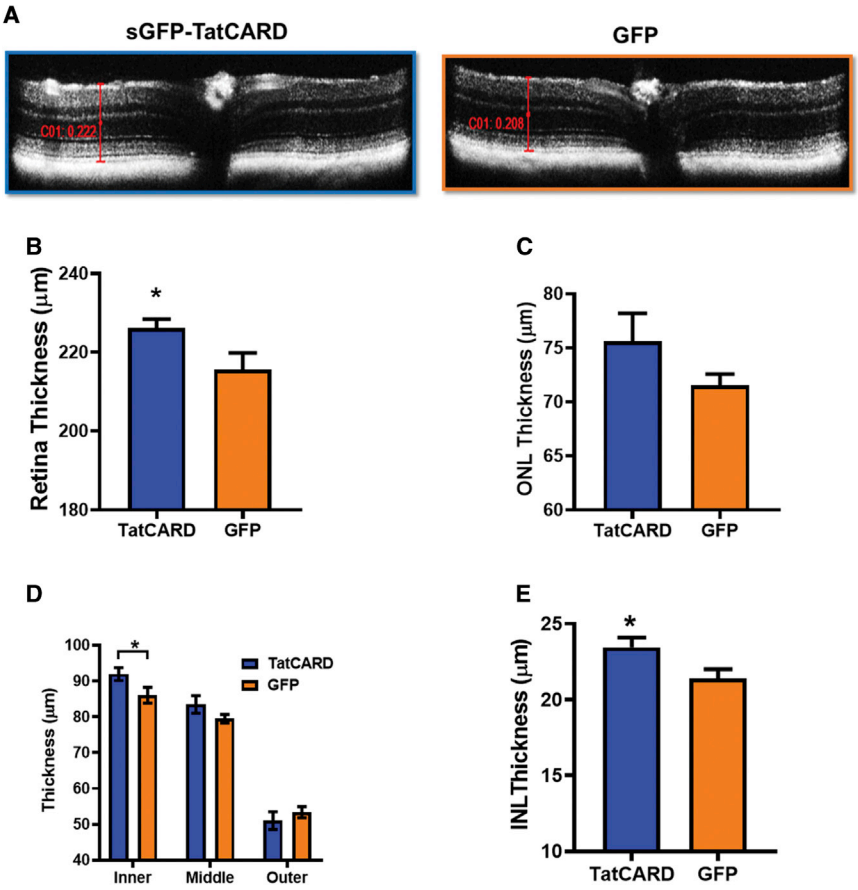

Figure 7. Expression of sGFP-TatCARD Maintains the Retinal Thickness of the RPE-Specific Sod2-Knockout Mouse Model of GA

Sod2floxed::VMD2Cre+ mice treated with AAV2quad (Y-F) + T491V vector delivering either sGFP-TatCARD or GFP were evaluated by SD-OCT at 16 months of age. (A) Representative B-scans of eyes treated with sGFP-TatCARD or GFP. (B) Total retina thickness was averaged for all the animals in each group. (C) The thicknesses of the inner, middle, and outer retina from each B-scan were measured using the Bioptigen Diver software. Thicknesses of the (D) inner nuclear layer (INL) and (E) outer nuclear layer (ONL) were also measured in B-scan images. Average ± SEM values for each group are reported. *$p \leq 0.05$, n = 9 mice.

(such as in RP) or multifactorial as in AMD. For these diseases, gene therapy would require the development of several vectors, each targeting a genetic defect associated with the disease; but, the targets will not be the same for all the patients with the same disease phenotype. To develop a gene-independent therapy, we propose targeting events such as inflammatory signals that take place in many retinal degenerative diseases.

The upregulation of the inflammasome pathway genes has also been detected in late stages of canine models of RP.[1] This observation indicates that, in advanced stages of RP, pro-inflammatory signals play an important role in the further degeneration of the retina. Since our vector targets caspase-1, which is a critical pro-inflammatory caspase, it holds great potential for controlling late stages of both age-related and mongenically inherited retinal degeneration.

MATERIALS AND METHODS

Chemicals

The sodium iodate (S4007-100G) was purchase from Sigma-Aldrich (St. Louis, MO, USA). The Nova Factor reagent (R-0003-01) was purchased from Venn Nova (Pompano Beach, FL, USA). Both the control siRNA (sc-37007) and the SOD2 siRNA pool (sc-41655) were purchased from Santa Cruz Biotechnology (Dallas, TX, USA).

Cell Culture

ARPE-19 cells were purchased from ATCC repository, and frozen stocks were prepared immediately. They were used at passages 1–9. Cells were grown in DMEM/F-12 medium containing 10% fetal bovine serum (FBS) and 1% penicillin and streptomycin.

Transfection of ARPE-19 Cells

ARPE-19 cells were plated in a 6-well plate at 8×10^5 cells/well in 3 mL DMEM/F12 supplemented with 10% FBS and 1% penicillin and streptomycin (Pen and Strep). Cells were kept for 24 h at 37°C with 5% CO_2. The growth medium was replaced with 2 mL DMEM/F12 without FBS or Pen and Strep, and cells were returned to the incubator. The siRNA-Nova Factor complexes of SOD2 siRNA and Ctrl siRNA were made by diluting 40 µL of either siRNA in 100 µL Optimem-I in 1.5-mL microcentrifuge tubes in a biological cabinet using sterile techniques. A total of 10 µL Nova Factor was diluted in 100 µL Optimem-I. This mixture was incubated at room temperature for 5 min. Afterward, the diluted Nova Factor was added to the corresponding siRNA and mixed by pipetting. Complexes were incubated at room temperature for 15 min. Complexes were added dropwise to the corresponding wells (three wells for SOD2 siRNA and three for Ctrl siRNA), and the plate was tilted several times to ensure proper distribution of the complexes. Cells were returned to the incubator, and the media were replaced the next day with 3 mL complete media. At 48 h after transfection, cells were harvested by trypsinization and centrifugation at 5,000 × *g* for 5 min at 4°C.

Western Blot

Cells were homogenized in cold NP-40 lysis buffer (1% NP-40, 150 mM NaCl, and 50 mM Tris-HCl [pH 8.0]) supplemented with 1× Halt Protease inhibitor cocktail (Thermo Fisher Scientific, Waltham, MA, USA) and 2 mM EDTA, and they were lysed with 30 strokes of a motorized pestle. Lysate was centrifuged at 14,000 × *g*

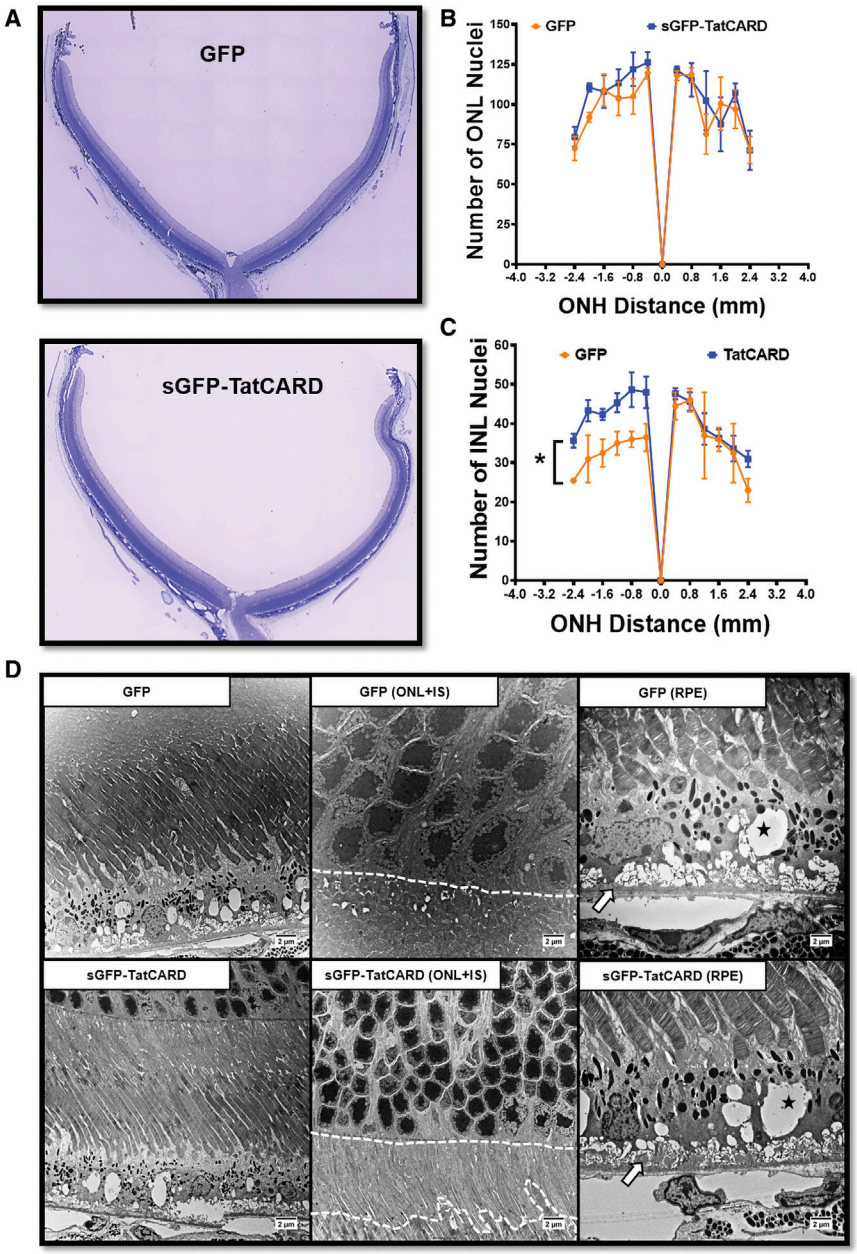

Figure 8. Retinal Expression of TatCARD after Intravitreal Administration Protects the Second-Order Neuron Nuclei and Not the Number of Surviving Photoreceptors in the SOD2-KO Mouse Model of GA

The eyes of 18-month-old SOD2-KO mice treated with AAV2quad(Y-F) + T491V delivering either GFP or sGFP-TatCARD were harvested after cardiac perfusion with a solution of glutaraldehyde and paraformaldehyde. Plastic thin sections were prepared and stained with toluidine blue to visualize nuclear layers. Sections were imaged using a bright-field microscope. (A) Representative images from GFP- and sGFP-TatCARD-treated eyes. (B and C) The numbers of (B) ONL nuclei and (C) INL nuclei were quantified using ImageJ software. No statistically significant difference in the number of ONL nuclei was observed between eyes treated with GFP or sGFP-TatCARD-delivering vector. However, the number of INL nuclei was statistically significantly greater in the TatCARD-treated eyes when compared to the GFP-treated eyes in the inferior retina. (D) Electron microscopy micrographs of 18-month-old sGFP-TatCARD-treated retinas had more organized photoreceptor inner segments when compared to GFP-treated retinas. RPE vacuoles (stars) and basal laminar deposits (arrows) were present in both GFP- and sGFP-TatCARD-treated retinas. Average ± SEM values for each group are reported. *$p \leq 0.05$, n = 2–3 eyes.

for 10 min at 4°C. Clear lysate was transferred to a new 1.5-mL tube. The protein concentration was determined as described below. Then 4 vol lysate was mixed with 1 vol 5× Laemmli buffer[37] containing DTT, and samples were boiled for 5 min. A total of 20 μg total protein was loaded onto a 12% SDS-PAGE gel and run at 100 V for 30 min. Gel was transferred into a polyvinylidene fluoride (PVDF) membrane using the iBind system (Invitrogen), as per the manufacturer's protocol. The membrane was then blocked with Odyssey blocking buffer for 1 h at room temperature with constant shaking. The membrane was then incubated overnight at 4°C with constant shaking with anti-SOD2 and anti-alpha-tubulin diluted in blocking buffer with 0.1% Tween-20. The next day, the membrane was washed 3 times (5 min/wash) with PBS-T (0.1% Tween-20 in 1× PBS) (Table 1). The membrane was then incubated with anti-mouse-680CDW and anti-rabbit-800CDW antibodies diluted in Odyssey blocking buffer with 0.1% Tween-20 for 45 min at room temperature with constant shaking. Afterward, the membrane was washed three times as described earlier and scanned using an Odyssey CLx scanner.

Sod2 Deletion Model

Our use of mice adhered to the guidelines of the Association for Research in Vision and Ophthalmology (ARVO) statement for the Use of Animals in Ophthalmic and Vision Research, and it was approved by the University of Florida Institutional Animal Care and Use Committee. These mice were transgenic for PVMD2-rtTA and tetO-PhCMVcre, and they were homozygous for *Sod2*-containing loxP sites surrounding exon 3. Breeders were screened for the absence of *rd1* and *rd8* mutations and for the RPE65 Met430 allele. Expression of Cre recombinase was induced by the feeding of doxycycline-containing chow to nursing dams for 2 weeks immediately after the birth of pups, as described by Mao et al.[26] Importantly, treatment with doxycycline was stopped several months before the analysis of retinal function or measurements of cytokines.[35–37]

Table 1. Antibodies Used in This Study

Antibody	Company	Catalogue Number	Dilution
ZO-1	Invitrogen	61-7300	1/50
SOD2	Abcam	ab13533	1/5,000
GFAP	Abcam	ab53554	1/500
IL-1b	Santa Cruz Biotechnology	sc-7884	1/1,000
Iba1	Wako	019-19741	1/1,000
Alpha-tubulin	Millipore	04-1117	1/5,000

Intravitreal Injection of AAV

The eyes of C57BL/6J mice between 8 and 10 weeks of age were dilated using ophthalmic solutions of atropine (1%) and phenylephrine (2.5%). Mice were anesthetized with a ketamine-xylazine mixture (100 mg/kg ketamine:4 mg/kg xylazine). A drop of proparacaine hydrochloride ophthalmic solution (0.5%) was added to the eye as topical anesthetic. An incision was made in the limbus region using a 27G needle, followed by the insertion of a Hamilton syringe with a 33G needle. Once inside the vitreous, as observed through a Leica stereoscope, 1 μL of the appropriate AAV was injected. Afterward the needle was retracted, and mice received an intraperitoneal injection of Antisedan (0.25 mg/kg) and topical antibiotics on the injection site. Mice were placed on a warm pad until ambulatory before being returned to their housing rack.

Sodium Iodate Mouse Model

C57BL/6J mice between 8 and 10 weeks old were injected intraperitoneally with 25 mg/kg sodium iodate in sterile saline a month after vector injection. These mice were evaluated at 7, 14, and 30 days after intraperitoneal (i.p.) injection by electroretinogram.

SD-OCT

Mice eyes were dilated with topical atropine and epinephrine solutions and anesthetized with a ketamine-xylazine mixture (100 mg/kg ketamine:4 mg/kg xylazine) given i.p. Anesthetized mice were placed on a platform and restrained in place. Using Bioptigen SD-OCT equipment, a total of 250 B-scans centered on the optic nerve head was obtained. Afterward, mice receive an i.p. injection of Antisedan (0.25 mg/kg) and were kept on a heated pad until ambulatory. Scans were averaged into 25 B-scans that were subjected to auto-segmentation using the Diver Software from Bioptigen.

ERG

Mice were dark adapted overnight. The next morning, mice eyes were dilated with eye drops of atropine and epinephrine, as described earlier. After being anesthetized as described earlier, mice were placed on a platform and electrodes were placed on their mouth, tail, and corneas. Corneal electrodes were adjusted until similar impedance values (<10 μV) were determined for both eyes, while mouth and tail impedance were both <16 μV. Mice were then subjected to three flashes of 20 cd/m^2 separated by 2-min intervals using a full-field dome. After the last recording, values were averaged and the a-, b-, and c-wave amplitudes were determined. Finally, mice received an i.p. injection of Antisedan as described earlier.

Protein Lysate Preparation

Cells were harvested and homogenized in 200 μL cold NP-40 lysis buffer (150 mM NaCl, 50 mM Tris-Cl [pH 8.0], and 1.0% NP-40) supplemented with 2 mM EDTA and 1× protease inhibitor cocktail (Roche), using a motorized pestle with 30 strokes. Cell homogenate was centrifuged at 14,000 × *g* for 5 min at 4°C. Clear lysate was collected in a new 1.5-mL microcentrifuge tube.

Protein Concentration Assay

Protein concentration was determined using the Bradford Assay from Bio-Rad. Briefly, BSA concentration was determined with a nanospectrophotometer. Standard was diluted into 1.5, 1.2, 0.9, 0.6, and 0.3 μg/μL using NP-40 lysis buffer. Reagent A from the kit was mixed with reagent S, as indicated by the company's protocol to make reagent A'. A total of 25 μL A' was added to each well followed by the addition of 5 μL sample. A total of 200 μL reagent B was added to each well using a multichannel pipette, followed by a 15-min incubation at room temperature with constant shaking. Absorbance at 750 nm was determined using a plate reader. Absorbance of blank wells was subtracted from all standards and samples. Sample concentrations were extrapolated from a linear regression generated using the BSA standards.

Multiplex ELISA

Retinas were homogenized in 200 μL NP-40 lysis buffer with 1× Halt's Protease Inhibitor Cocktail (Thermo Fisher Scientific, Waltham, MA, USA), using 30 strokes of a motorized pestle (Sigma-Aldrich, St. Louis, MO, USA). The protein concentration was determined with the Pierce 660 nm Protein Assay Reagent (Thermo Fisher Scientific, Waltham, MA, USA), as per the manufacturer's protocol. Homogenates were diluted to 0.89 μg/μL in a total volume of 100 μL using PBS 1×. The MILLIPLEX MAP Kit (Millipore, Burlington, MA, USA) purchased for the Mouse Cytokine and Chemokine Magnetic Bead Panel was MCYTOMAG-70K. The mouse cytokine standard 6 and quality controls 1 and 2 were prepared by resuspending in 250 μL deionized water. The working standards were prepared by adding 200 μL assay buffer to 5 tubes. A serial dilution was performed by adding 50 μL standard 6 to the standard 5 tube and so on.

The Mouse Cytokine and Chemokine Magnetic Bead Panel plate was prepared by washing it with 200 μL wash buffer, and it was shaken vigorously for 10 min. The wash buffer was decanted and the residual buffer was removed by lightly tapping the plate on an absorbent towel. 25 μL standards and quality controls were added in duplicates to the appropriate wells. Assay buffer was used as the blank standard. 25 μL assay buffer was added to all the sample wells, standards, and quality controls. 25 μL of each sample was added in duplicates to the appropriate wells. The Antibody-Immobilized Pre-mixed Beads were prepared by sonicating the bottle for 30 s and then vortexing the bottle for 1 min. After vortexing, 25 μL pre-mixed beads was added to

each well. The beads were mixed intermittently by vortexing after every column. The plate was sealed with a foil plate sealer and incubated at 4°C overnight with agitation on a plate shaker.

The next day, the well contents were removed by placing the plate on a Magnetic 96-well plate Separator (Millipore, Burlington, MA, USA) for 1 min to allow the magnetic particles to remain bound. 200 μL wash buffer was added to the plate and shaken vigorously for 30 s, placed on the magnetic plate for 1 min, and then decanted. This step was repeated for a total of two times. After the detection antibodies reached room temperature, 25 μL was added to each well containing the standards, the quality controls, and the samples. The plate was sealed with a foil plate sealer and incubated at room temperature with agitation on a plate shaker for 1 h. A total of 25 μL Streptavidin-Phycoerythin was added to each well that contained the 25 μL detection antibody. The plate was sealed with a foil plate sealer and incubated at room temperature with agitation on a plate shaker for 30 min. The plate was placed on the magnetic plate for 1 min to allow the magnetic particles to remain bound and then decanted. 200 μL wash buffer was added to the plate and shaken vigorously for 30 s, placed on the magnetic plate for 1 min, and then decanted. This step was repeated for a total of two times. 150 μL wash buffer was added to all the wells containing the standards, the quality controls, and the samples. The plate was analyzed on MAGPIX with Xponent Software (Millipore, Burlington, MA, USA). A total of 150 beads/region was acquired per each well.

Quantification of Nuclei in Plastic Sections Using ImageJ

Sections were imaged using a Leica wide-field microscope and the LAX software. Images were generated using 20× magnification images tiled using a computer algorithm. Images were opened in ImageJ and calibrated using a 3.3 pixel/μm ratio (83.304 pixels = 25 μm). The upper or lower retina was selected using the segmented line option with a 900-μm thickness. The section was then straightened using this option under the selection section. Brightness and contrast were auto-adjusted, and a grid was placed on the image (Analyze → Tools → Grid). Quadrants at every 400 μm from the optic nerve head (ONH) were identified and selected using the square selection tool. Selected areas were duplicated, and the new image was labeled with the distance from the ONH. The image was then converted to an 8-bit image, and the black and white threshold was adjusted to only show the nuclei present in the image. Nuclei were quantified using the particle analyzer option under Analyze using the following parameters: Size, 3-Infinity; Circularity, 0.00–1.00; Show, Outlines, select summarize and exclude on edges. The outlined image was used to confirm that the number of identified nuclei agreed with the figure being counted.

Statistical Analysis

Data from *in vitro* experiments were analyzed by Student's t test. *In vivo* studies were analyzed by paired Student's t test, except for experiments in which samples came from different animals, which were analyzed by unpaired Student's t test. A difference was considered significant at $p \leq 0.05$. Data were graphed using GraphPad Prism 8 software (La Jolla, CA, USA).

SUPPLEMENTAL INFORMATION

Supplemental Information can be found online at https://doi.org/10.1016/j.omtm.2019.06.001.

AUTHOR CONTRIBUTIONS

B.M.Y. conducted experiments and analyzed data. K.J. conducted experiments. M.T.M. conducted experiments and analyzed data. E.W. and H.L. conducted experiments. A.S.L. provided scientific input and prepared the manuscript. C.J.I. conducted experiments, analyzed data, supervised experiments, and prepared the manuscript.

ACKNOWLEDGMENTS

This work was supported by a grant from the National Eye Institute (R01EY026268), a research grant from the Bright Focus Foundation (M2017126), and an unrestricted grant from Research to Prevent Blindness, Inc.

REFERENCES

1. Sudharsan, R., Beiting, D.P., Aguirre, G.D., and Beltran, W.A. (2017). Involvement of Innate Immune System in Late Stages of Inherited Photoreceptor Degeneration. Sci. Rep. *7*, 17897.

2. Feng, S., Yu, H., Yu, Y., Geng, Y., Li, D., Yang, C., Lv, Q., Lu, L., Liu, T., Li, G., and Yuan, L. (2018). Levels of Inflammatory Cytokines IL-1*β*, IL-6, IL-8, IL-17A, and TNF-*α* in Aqueous Humour of Patients with Diabetic Retinopathy. J. Diabetes Res. *2018*, 8546423.

3. Gao, J., Cui, J.Z., To, E., Cao, S., and Matsubara, J.A. (2018). Evidence for the activation of pyroptotic and apoptotic pathways in RPE cells associated with NLRP3 inflammasome in the rodent eye. J. Neuroinflammation *15*, 15.

4. Appelbaum, T., Santana, E., and Aguirre, G.D. (2017). Strong upregulation of inflammatory genes accompanies photoreceptor demise in canine models of retinal degeneration. PLoS ONE *12*, e0177224.

5. Pennington, K.L., and DeAngelis, M.M. (2016). Epidemiology of age-related macular degeneration (AMD): associations with cardiovascular disease phenotypes and lipid factors. Eye Vis. (Lond.) *3*, 34.

6. Yan, Q., Ding, Y., Liu, Y., Sun, T., Fritsche, L.G., Clemons, T., Ratnapriya, R., Klein, M.L., Cook, R.J., Liu, Y., et al.; AREDS2 Research Group (2018). Genome-wide analysis of disease progression in age-related macular degeneration. Hum. Mol. Genet. *27*, 929–940.

7. Cano, M., Thimmalappula, R., Fujihara, M., Nagai, N., Sporn, M., Wang, A.L., Neufeld, A.H., Biswal, S., and Handa, J.T. (2010). Cigarette smoking, oxidative stress, the anti-oxidant response through Nrf2 signaling, and Age-related Macular Degeneration. Vision Res. *50*, 652–664.

8. Nita, M., Grzybowski, A., Ascaso, F.J., and Huerva, V. (2014). Age-related macular degeneration in the aspect of chronic low-grade inflammation (pathophysiological parainflammation). Mediators Inflamm. *2014*, 930671.

9. Wang, Y., Hanus, J.W., Abu-Asab, M.S., Shen, D., Ogilvy, A., Ou, J., Chu, X.K., Shi, G., Li, W., Wang, S., and Chan, C.C. (2016). NLRP3 Upregulation in Retinal Pigment Epithelium in Age-Related Macular Degeneration. Int. J. Mol. Sci. *17*, E73.

10. Bhutto, I., and Lutty, G. (2012). Understanding age-related macular degeneration (AMD): relationships between the photoreceptor/retinal pigment epithelium/Bruch's membrane/choriocapillaris complex. Mol. Aspects Med. *33*, 295–317.

11. Chirco, K.R., Whitmore, S.S., Wang, K., Potempa, L.A., Halder, J.A., Stone, E.M., Tucker, B.A., and Mullins, R.F. (2016). Monomeric C-reactive protein and inflammation in age-related macular degeneration. J. Pathol. *240*, 173–183.

12. Liu, W., Gu, J., Qi, J., Zeng, X.-N., Ji, J., Chen, Z.-Z., and Sun, X.L. (2015). Lentinan exerts synergistic apoptotic effects with paclitaxel in A549 cells via activating ROS-TXNIP-NLRP3 inflammasome. J. Cell. Mol. Med. *19*, 1949–1955.

13. Feng, H., Gu, J., Gou, F., Huang, W., Gao, C., Chen, G., Long, Y., Zhou, X., Yang, M., Liu, S., et al. (2016). High Glucose and Lipopolysaccharide Prime NLRP3 Inflammasome via ROS/TXNIP Pathway in Mesangial Cells. J. Diabetes Res. *2016*, 6973175.

14. Chen, W., Zhao, M., Zhao, S., Lu, Q., Ni, L., Zou, C., Lu, L., Xu, X., Guan, H., Zheng, Z., and Qiu, Q. (2017). Activation of the TXNIP/NLRP3 inflammasome pathway contributes to inflammation in diabetic retinopathy: a novel inhibitory effect of minocycline. Inflamm. Res. *66*, 157–166.

15. Lu, A., Magupalli, V.G., Ruan, J., Yin, Q., Atianand, M.K., Vos, M.R., Schröder, G.F., Fitzgerald, K.A., Wu, H., and Egelman, E.H. (2014). Unified polymerization mechanism for the assembly of ASC-dependent inflammasomes. Cell *156*, 1193–1206.

16. Ildefonso, C.J., Jaime, H., Biswal, M.R., Boye, S.E., Li, Q., Hauswirth, W.W., and Lewin, A.S. (2015). Gene therapy with the caspase activation and recruitment domain reduces the ocular inflammatory response. Mol. Ther. *23*, 875–884.

17. Kay, C.N., Ryals, R.C., Aslanidi, G.V., Min, S.H., Ruan, Q., Sun, J., Dyka, F.M., Kasuga, D., Ayala, A.E., Van Vliet, K., et al. (2013). Targeting photoreceptors via intravitreal delivery using novel, capsid-mutated AAV vectors. PLoS ONE *8*, e62097.

18. Machalińska, A., Lubiński, W., Kłos, P., Kawa, M., Baumert, B., Penkala, K., Grzegrzółka, R., Karczewicz, D., Wiszniewska, B., and Machaliński, B. (2010). Sodium iodate selectively injuries the posterior pole of the retina in a dose-dependent manner: morphological and electrophysiological study. Neurochem. Res. *35*, 1819–1827.

19. Seo, S.J., Krebs, M.P., Mao, H., Jones, K., Conners, M., and Lewin, A.S. (2012). Pathological consequences of long-term mitochondrial oxidative stress in the mouse retinal pigment epithelium. Exp. Eye Res. *101*, 60–71.

20. Sorsby, A. (1941). EXPERIMENTAL PIGMENTARY DEGENERATION OF THE RETINA BY SODIUM IODATE. Br. J. Ophthalmol. *25*, 58–62.

21. Berkowitz, B.A., Podolsky, R.H., Lenning, J., Khetarpal, N., Tran, C., Wu, J.Y., Berri, A.M., Dernay, K., Shafie-Khorassani, F., and Roberts, R. (2017). Sodium Iodate Produces a Strain-Dependent Retinal Oxidative Stress Response Measured In Vivo Using QUEST MRI. Invest. Ophthalmol. Vis. Sci. *58*, 3286–3293.

22. Chowers, G., Cohen, M., Marks-Ohana, D., Stika, S., Eijzenberg, A., Banin, E., and Obolensky, A. (2017). Course of Sodium Iodate-Induced Retinal Degeneration in Albino and Pigmented Mice. Invest. Ophthalmol. Vis. Sci. *58*, 2239–2249.

23. Hanus, J., Anderson, C., Sarraf, D., Ma, J., and Wang, S. (2016). Retinal pigment epithelial cell necroptosis in response to sodium iodate. Cell Death Discov. *2*, 16054.

24. Kosmidou, C., Efstathiou, N.E., Hoang, M.V., Notomi, S., Konstantinou, E.K., Hirano, M., Takahashi, K., Maidana, D.E., Tsoka, P., Young, L., et al. (2018). Issues with the Specificity of Immunological Reagents for NLRP3: Implications for Age-related Macular Degeneration. Sci. Rep. *8*, 461.

25. Bian, Z.-M., Field, M.G., Elner, S.G., Kahlenberg, J.M., and Elner, V.M. (2018). Distinct CD40L receptors mediate inflammasome activation and secretion of IL-1β and MCP-1 in cultured human retinal pigment epithelial cells. Exp. Eye Res. *170*, 29–39.

26. Mao, H., Seo, S.J., Biswal, M.R., Li, H., Conners, M., Nandyala, A., Jones, K., Le, Y.Z., and Lewin, A.S. (2014). Mitochondrial oxidative stress in the retinal pigment epithelium leads to localized retinal degeneration. Invest. Ophthalmol. Vis. Sci. *55*, 4613–4627.

27. Biswal, M.R., Ildefonso, C.J., Mao, H., Seo, S.J., Wang, Z., Li, H., Le, Y.Z., and Lewin, A.S. (2016). Conditional Induction of Oxidative Stress in RPE: A Mouse Model of Progressive Retinal Degeneration. Adv. Exp. Med. Biol. *854*, 31–37.

28. Wu, J., Peachey, N.S., and Marmorstein, A.D. (2004). Light-evoked responses of the mouse retinal pigment epithelium. J. Neurophysiol. *91*, 1134–1142.

29. Biswal, M.R., Han, P., Zhu, P., Wang, Z., Li, H., Ildefonso, C.J., and Lewin, A.S. (2017). Timing of Antioxidant Gene Therapy: Implications for Treating Dry AMD. Invest. Ophthalmol. Vis. Sci. *58*, 1237–1245.

30. Camelo, S., Calippe, B., Lavalette, S., Dominguez, E., Hur, J., Devevre, E., Guillonneau, X., Raoul, W., and Sennlaub, F. (2015). Thinning of the RPE and choroid associated with T lymphocyte recruitment in aged and light-challenged mice. Mol. Vis. *21*, 1051–1059.

31. Lobanova, E.S., Finkelstein, S., Li, J., Travis, A.M., Hao, Y., Klingeborn, M., Skiba, N.P., Deshaies, R.J., and Arshavsky, V.Y. (2018). Increased proteasomal activity supports photoreceptor survival in inherited retinal degeneration. Nat. Commun. *9*, 1738.

32. Dexter, P.M., Lobanova, E.S., Finkelstein, S., Spencer, W.J., Skiba, N.P., and Arshavsky, V.Y. (2018). Transducin β-Subunit Can Interact with Multiple G-Protein γ-Subunits to Enable Light Detection by Rod Photoreceptors. eNeuro *5*, ENEURO.0144-18.2018.

33. Xiao, J., Yao, J., Jia, L., Lin, C., and Zacks, D.N. (2017). Protective Effect of Met12, a Small Peptide Inhibitor of Fas, on the Retinal Pigment Epithelium and Photoreceptor After Sodium Iodate Injury. Invest. Ophthalmol. Vis. Sci. *58*, 1801–1810.

34. Doyle, S.L., Campbell, M., Ozaki, E., Salomon, R.G., Mori, A., Kenna, P.F., Farrar, G.J., Kiang, A.S., Humphries, M.M., Lavelle, E.C., et al. (2012). NLRP3 has a protective role in age-related macular degeneration through the induction of IL-18 by drusen components. Nat. Med. *18*, 791–798.

35. Ramkumar, H.L., Zhang, J., and Chan, C.-C. (2010). Retinal ultrastructure of murine models of dry age-related macular degeneration (AMD). Prog. Retin. Eye Res. *29*, 169–190.

36. Pierce, E.A., and Bennett, J. (2015). The Status of RPE65 Gene Therapy Trials: Safety and Efficacy. Cold Spring Harb. Perspect. Med. *5*, a017285.

37. Laemmli, U.K. (1970). Cleavage of structural proteins during the assembly of the head of bacteriophage T4. Nature *227*, 680–685.